A Novel Dual Circulating Fluidized Bed System for Chemical Looping Processes

Tobias Pröll, Philipp Kolbitsch, Johannes Bolhàr-Nordenkampf, and Hermann Hofbauer
Vienna University of Technology, Institute of Chemical Engineering, 1060 Wien, Austria

DOI 10.1002/aic.11934
Published online August 13, 2009 in Wiley InterScience (www.interscience.wiley.com).

A fluidized bed system combining two circulating fluidized bed reactors is proposed and investigated for chemical looping combustion. Direct hydraulic communication of the two circulating fluidized bed reactors via a fluidized loop seal allows for high rates of global solids circulation and results in a stable solids distribution in the system. A 120 kW fuel power bench scale unit was designed, built, and operated. Experimental results are presented for natural gas as fuel using a nickel-based oxygen carrier. No carbon was lost to the air reactor under any conditions operated. It is shown from fuel power variations that a turbulent/fast fluidized bed regime in the fuel reactor is advantageous. Despite the relatively low riser heights (air reactor: 4.1 m, fuel reactor: 3.0 m), high CH_4 conversion and CO_2 yield of up to 98% and 94%, respectively, can be reported for the material tested. © 2009 American Institute of Chemical Engineers *AIChE J,* 55: 3255–3266, 2009

Keywords: fluidization, circulating fluidized bed, reactor system, combustion, chemical looping, carbon capture

Introduction

Chemical looping for carbon capture

Carbon capture and storage is the key mid-term strategy to limit the carbon dioxide concentration in the atmosphere. Different approaches are currently discussed in order to capture CO_2 from combustion processes. Most of these approaches require gas separation steps: either CO_2 separation (precombustion and postcombustion capture) or O_2 separation from air (oxyfuel combustion). Chemical looping combustion (CLC), however, is a method of indirect combustion where fuel and air are never mixed. The concept has therefore been classified as "unmixed combustion."[1] Metal oxides are used to selectively transport oxygen from air to fuel in the solid phase. If a suitable metal oxide is used as the oxygen carrier, the CLC system can be operated in such a way that the exhaust gas of the fuel reactor ideally consists of CO_2 and H_2O only and allows for subsequent water condensation, compression, and storage of CO_2. The costly gas–gas separation steps are inherently avoided. Therefore, CLC is discussed as one of the most energy-efficient approaches to carbon capture from power production or fuel upgrading.[2]

Since 2000, CLC has received increasing attention. Most of the research is focused on particle development and reactivity testing of oxygen carriers in the laboratory or in small batch-type fluidized bed reactors.[3] Several groups around the world operate continuous looping installations of limited size.[4–7] These installations are used to test continuous operability and long-term stability. The reactor systems seem to be optimized for compact and convenient laboratory testing. On the other hand, there is only a limited focus on scalability to industrial size. Most of the small units need to be electrically heated to maintain the operating temperature. There are oxygen carriers available today that perform satisfactorily with respect to fuel conversion. Therefore, apart from further improvement of particles, optimization of CLC reactor systems suitable for scale-up turns out to be a second important task that is gaining importance in technology development.

Chemical looping state of the art

Although other concepts such as moving bed reactors have been proposed and investigated,[8] chemical looping

Correspondence concerning this article should be addressed to T. Pröll at tobias.proell@tuwien.ac.at

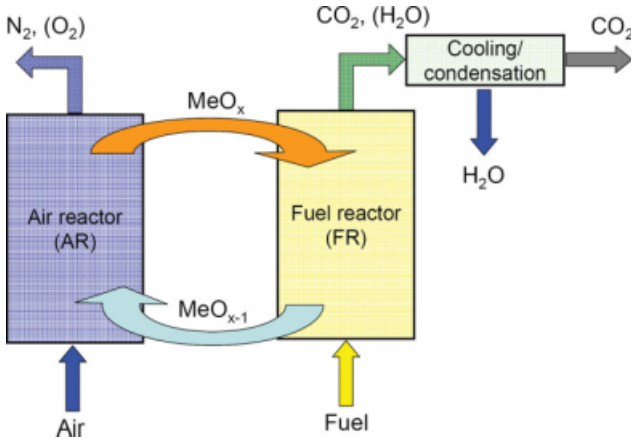

Figure 1. Chemical looping combustion.

[Color figure can be viewed in the online issue, which is available at www.interscience.wiley.com.]

combustion is a typical dual fluidized bed technology where chemically active bed material, that is metal oxide, is circulated between two fluidized bed reactors that are separated with respect to the gas phase (Figure 1). It was initially proposed in 1954 as a method to produce pure CO_2 from oxidizable carbonaceous material.[9] Then, the concept was studied theoretically as a means to improve the reversibility of combustion.[10–12] CLC has since then been identified as a promising technology for CO_2 capture from power plants, where 100% carbon capture can be achieved without a significant energy penalty.[13–18] In the so-called fuel reactor, a hydrocarbon fuel is oxidized by oxygen released from the bed material. The global reaction in the fuel reactor can be summarized for the case of full oxidation as follows:

$$C_xH_y + \left(2x + \frac{y}{2}\right)MeO_\alpha \rightarrow xCO_2 + \frac{y}{2}H_2O + \left(2x + \frac{y}{2}\right)MeO_{\alpha-1} \quad (1)$$

This step takes place at temperatures between 1000 and 1250 K and is either slightly exothermic or even endothermic depending on the type of fuel and on the oxygen carrier chosen. In the so-called air reactor, the bed material is reoxidized with air:

$$MeO_{\alpha-1} + \frac{1}{2}O_2 \rightarrow MeO_\alpha \quad (2)$$

This step is always strongly exothermic and the sum of reaction enthalpies of Reactions (1) and (2) is equal to the reaction enthalpy of direct combustion. Heat is withdrawn from the system with the hot exhaust gas streams. For common excess air ratios around 1.2, additional heat must be withdrawn directly from the reactors either by cooling the reactor walls or by cooling the circulating bed material stream. In practice, the extent to which fuel oxidation happens in the fuel reactor depends on the availability of oxygen (sufficient carrier circulation), on the thermodynamic properties of the oxygen carrier, and on the kinetics of the elementary gas–solid reactions (sufficient gas–solid contact time). If less oxygen is provided than is needed for full oxidation, the chemical looping system operates in chemical looping reforming (CLR) mode. In this case the fuel reactor exhaust contains at least the combustible species CO and H_2 besides CO_2 and H_2O and the global heat release is decreased.

A key issue for the industrial feasibility of CLC is the availability of oxygen carriers that are suitable from both the technical and the economical perspectives. Oxygen carriers should be capable of high fuel conversion from the thermodynamics perspective, have high reactivity with fuel and oxygen, sufficient oxygen carrier capacity (to limit the necessary solids circulation), and high mechanical stability for use in fluidized beds, and should be cheap as well as environmentally sound. Metal oxides such as Fe_2O_3, NiO, CuO, and Mn_3O_4 on an inert material such as Al_2O_3, TiO_2, and/or ZrO_2 are the most promising candidates today. Apart from designed particles, natural or waste materials have been found suitable especially for syngas conversion and in combination with solid fuels.[19] Extensive research is performed concerning the selection, preparation, and subsequent testing of materials as summarized, for example, by Johansson et al.[20] and Lyngfelt et al.[21]

At Chalmers University of Technology a chemical looping combustion installation is successfully operated at a scale of 10 kW fuel power.[4] This installation works according to the concept shown in Figure 2, with the air reactor as a circulating fluidized bed riser and the fuel reactor as a bubbling bed reactor in the return loop of the solids, separated from the riser by moderately fluidized loop seals. In terms of the principle, such a configuration is also successfully used for biomass gasification at a scale of 8 MW fuel power.[22]

Keeping in mind the discussed size of carbon capture plants of several hundreds of megawatts, the bubbling fluidized bed approach for the fuel reactor may not be economically feasible because of the tremendous bed surfaces required for this design.[23] Not only because of this, but also

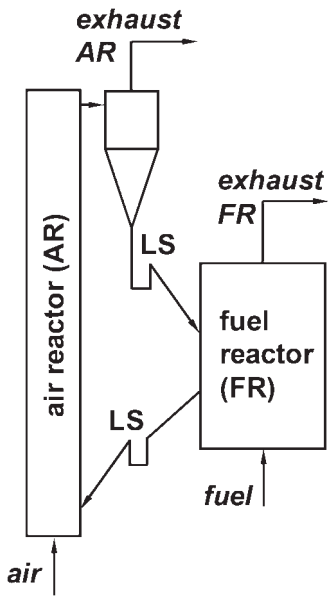

Figure 2. Structure of the 10 kW chemical looping unit at Chalmers University of Technology (according to Lyngfelt and Thunman,[4] LS = loop seal).

Table 1. Dual Fluidized Bed Technologies Apart from FCC

Technology	Purpose of Solids	Importance of Gas–Solid Contact	References
(Biomass) gasification	Heat transport, catalyst	Partially for tar reforming in the gas generator	25–29
Sorption enhanced reforming	CO_2 and heat transport, catalyst	High in the reformer/carbonator, low in the re-calciner (heat-driven)	30–35
Carbonate looping for CO_2 capture	CO_2 (and heat) transport	High in the absorber/carbonator, low in the re-calciner (heat-driven)	36–40
Chemical looping	Oxygen and heat transport	High in both reactors, no gas phase conversion without solids	4–7, 41–44

because increased gas–solid interaction is expected in the turbulent or fast fluidized regime,[24] the unit investigated in the present study consists of two interconnected circulating fluidized bed reactors.

The Dual Circulating Fluidized Bed Concept

Dual fluidized bed systems

The general idea with dual fluidized bed (DFB) reactor systems is to expose two different gas streams to a circulating stream of solids transporting heat and often also, in a selective way, chemical species. The use of loop seals fluidized with inert gases avoids direct contact between the two main gas streams. The classical application of this concept is the fluid catalytic cracking process (FCC), where carbon depositions on catalyst particles are combusted in a second reaction zone. Along with the progress in energy conversion technology, several technologies other than FCC but based on the DFB approach have been proposed and have partly been successfully demonstrated. A brief overview is given in Table 1.

With respect to the necessary interaction of gases and solids in the system, chemical looping processes in particular require high gas–solid interaction and sufficient contact time in both reactors.

Systems combining two CFB reactors

Systems combining two CFB reactors have already been proposed for biomass steam gasification[27] and chemical looping processes.[41–43] The principal schemes of these concepts are sketched in Figure 3. In both systems, the solids must pass a cyclone at least twice during one entire loop. The entrainment of both risers is crucially necessary in order to provide circulation of solids between the two reactors. In the case of the system in Figure 3b, partial back mixing of solids is possible on either side. For the two-way loop seals, measures need to be taken in order to control the flow rate of solids going into each of the two loop seal outlets. In case the process requires high global circulation, such a back mixing loop means a higher solids load on the cyclones compared to the case without a solids flow back into the same reactor.

The DCFB system

For chemical looping combustion (CLC) or reforming (CLR) processes with selective oxygen transport by the bed material, the following basic requirements can be stated:

- A high rate of global solids circulation is required in order to provide enough oxygen in the fuel reactor.
- Excellent gas–solids contact is required in both reactors in order to obtain satisfactory gas conversion. This is especially true for the fuel reactor of CLC systems where significant amounts of unconverted fuel will hardly be tolerable in applications.

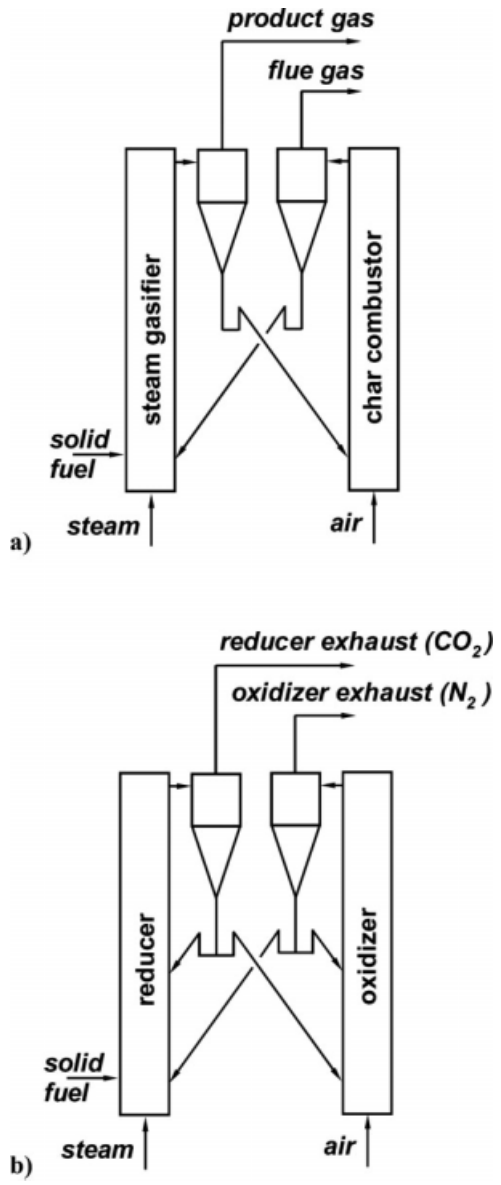

Figure 3. Systems featuring two circulating fluidized bed reactors: (a) Battelle/FERCO biomass gasifier,[27] (b) Alstom chemical looping reactor concept.[43]

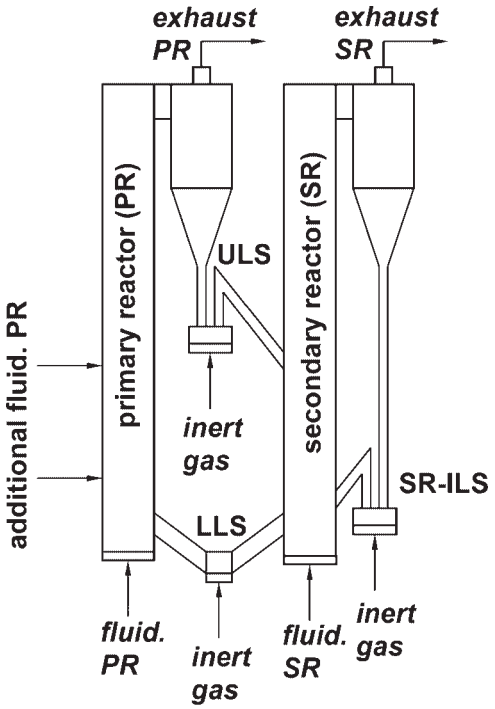

Figure 4. Dual circulating fluidized bed reactor system (LLS = lower loop seal, ULS = upper loop seal, SR-ILS = secondary reactor internal loop seal).

• Low particle attrition rates are appreciated especially if costly oxygen carriers are to be used.

Therefore, the system investigated in the present study represents a combination of the existing practice in CLC technology according to Figure 2 with the idea of using two scale-up ready CFBs for both air reactor and fuel reactor. A second aim of the present effort is to propose a robust fluidized bed system which is most simple with respect to necessary process control devices. In the dual circulating fluidized bed (DCFB) system according to Figure 4, the two CFB reactors are interconnected via a fluidized loop seal in the bottom region of the reactors (lower loop seal). The entrainment of the left-hand side reactor (primary reactor) determines global solids circulation. The solids are separated from the primary reactor exhaust stream in a cyclone separator and pass over through a fluidized loop seal (upper loop seal) into the right-hand side reactor (secondary reactor). From there, the global solids loop closes via the lower loop seal. The secondary reactor features a circulation loop in itself (secondary reactor cyclone and internal loop seal) and may be optimized with respect to good gas–solid contact and low particle attrition rates. The global circulation rate can be controlled by staged fluidization of the primary reactor. This is common practice in CFB technology. The direct hydraulic communication of the two CFB reactors allows stable solids distribution in the system as long as the lower loop seal is designed to be large enough to not significantly hinder solids flow. Imposing moderate pressure differences between the two reactors changes the theoretical solids levels in the system. This can be done by changing the backpressure from the exhaust gas lines, allowing active control of the solids hold-up in each reactor. A cold flow model of the DCFB unit described in this article has been operated prior to construction of the bench scale plant. The results show a high rate of global solids circulation between air reactor and fuel reactor. Staged fluidization of the air reactor allows active control of the global circulation. The pressure profiles measured in the cold flow model indicate a fast fluidized regime in the air reactor and a pronounced dense bottom region with a relatively lean upper zone in the fuel reactor.[45]

Apart from CLC, the DCFB system has the potential to be applied in other dual bed processes such as carbonate looping for end-of-pipe CO_2 capture, dual bed gasification, and sorption enhanced reforming.

Experimental

Design of the 120 kW unit

A DCFB test rig for CLC of gaseous fuels has been designed and built with the hot commissioning phase completed in early 2008. The air reactor (AR) of the CLC system is designed as the primary reactor in the sense of the DCFB concept described earlier. The fuel reactor (FR) is the secondary reactor, which may be optimized with respect to gas phase conversion. For the purpose of simplicity at the small scale, the lower loop seal connecting the two reactors represents a continuation of the reactor bodies. The main fluidization nozzles are arranged along the circumference of the cylindrical reactor shells. A sketch of the test rig is shown in Figure 5

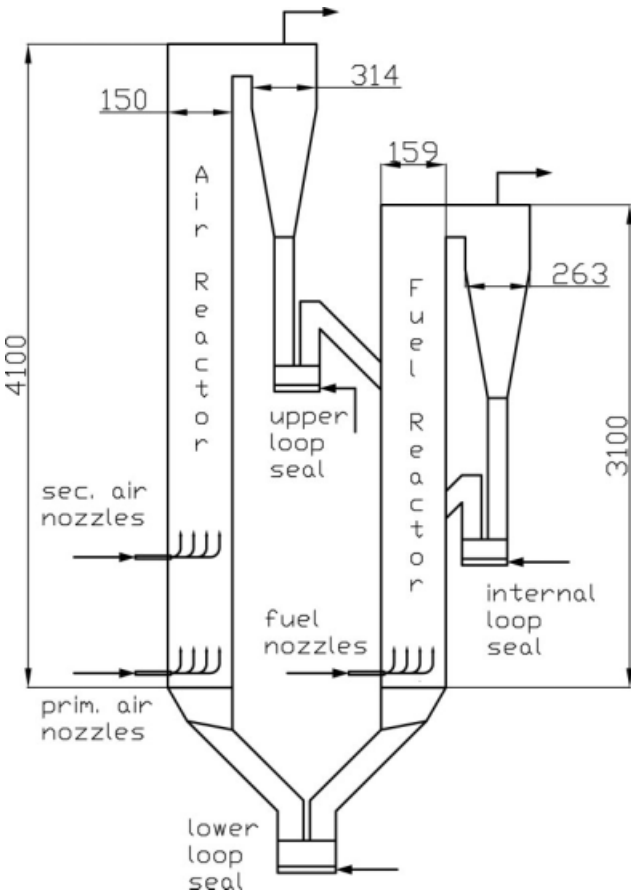

Figure 5. Sketch of the 120 kW bench scale DCFB unit.

Table 2. Bulk Geometry and Design Data of the 120 kW Unit

Parameter	Unit	Value AR	Value FR
Reactor inner diameter	m	0.150	0.159
Reactor height	m	4.1	3.0
Height of primary gas inlet	m	0.025	0.06
Height of secondary gas inlet	m	1.325	–
Inlet gas flow	Nm^3/h	138.0	12.0
Outlet gas flow	Nm^3/h	113.9	35.9
Temperature in reactor	K	1213	1123
Design fluid for calculation		depleted air	$H_2O/CO_2 = 2/1$
Mean particle size	mm	0.12	
Particle apparent density	kg/m^3	3200	
Particle sphericity	–	0.99	
Archimedes number	–	7.55	9.13
Superficial velocity	m/s	7.32	2.08
Ratio U/U_{mf}	–	1280.4	315.4
Ratio U/U_t	–	15.5	3.8
Fuel power (natural gas)	kW	120	
Lower heating value of fuel	MJ/kg	48.8	
Design air/fuel ratio	–	1.2	

with the most important geometric data and other design parameters summarized in Table 2. More information on the design of the unit has been reported by Kolbitsch et al.[46] and a mathematical model of the DCFB unit including gas–solid reaction kinetics has been presented by Kolbitsch et al.[23]

Figure 6 shows the fluidization regimes of the design case operating points for both air reactor and fuel reactor. The design of the fuel reactor focuses on the gas–solids contact and solids inventory of the reactor. By applying a turbulent fluidized bed in the fuel reactor, the reactor size, solids inventory, and potential slip of unconverted fuel in the bubble phase are reduced. According to Bi and Grace,[47] a turbulent regime in a fluidized bed is defined in the range $U_c < U < U_{se}$, with U_c being the superficial velocity at the point where the standard deviation of differential pressure fluctuations reaches a maximum. For the chosen oxygen carrier, this region is very narrow and it is not possible to stay inside the limits in different operation cases. Therefore, the superficial gas velocity has been set slightly below the turbulent region in Figure 6.

Plant equipment and arrangement

To remove the heat released from combustion and to control the system temperature independently of the global air ratio, the air reactor shell is equipped with three cooling jackets covering most of the reactor height. These cooling jackets are operated with air and steam as cooling media. The cyclone separators are designed according to Hugi and Reh.[48] Apart from natural gas from the Viennese grid (98.7 vol % CH_4), the unit can be operated with mixtures of CO, H_2, and N_2 as well as with propane from gas cylinders. The loop seals are fluidized with steam in nominal operation and may be switched to air fluidization during startup and shutdown. The exhaust gas streams of the two reactors are cooled separately to 550–600 K and analyzed online to evaluate the conversion of the fuel as well as the leakages of the loop seals. For the fuel reactor exhaust gas composition, a Rosemount NGA 2000 (CO: 0–100%, CO_2: 0–100%, O_2: 0–25%, H_2: 0–100%, CH_4: 0–100%) is used and, additionally, an online gas chromatograph Syntech Spectras GC 955, which allows cross-checking of carbon species and determination of the N_2 content for evaluation of possible gas leakages from the air reactor to the fuel reactor. The air reactor exhaust stream is analyzed using a Rosemount NGA 2000 (CO: 0–100%, CO_2: 0–100%, O_2: 0–25%). The cooled exhaust gas streams pass valves which make it possible to impose a defined backpressure on each reactor. The exhaust gas streams are then mixed and sent to a natural gas-fired post combustion unit, cooled again, cleaned in a bag filter, and sent to the chimney. Solids sampling is possible via the upper and the lower loop seal during operation. This allows accurate interpretation of experimental results (degree of oxidation of carrier and solids circulation rate).[49] The plant is operated and monitored using computer-integrated process control. The flow rates of the two fluidizing air streams and the fuel stream are measured and controlled using rotary instruments (Elster Instromet RVG) in combination with electrical control valves. The steam flow rates to the loop seals are measured using industrial steam flow meters (Krohne H250/RR/M9). Temperature and system pressure are measured online at 30 positions. Pressure measurements allow online determination of the actual solids inventory in each reactor. For safe handling of potentially hazardous solids, a portable lock is used in combination with pneumatic transport lines.

Experimental procedure

The unit is started up using a 35 kW natural gas burner attached to the fuel reactor and a 15 kW electrical air preheater on the air reactor side. At the beginning, both reactors and all three loop seals are fluidized with air. Solids circulation is easily possible even in cold conditions, so the energy of the startup burner is distributed by the heated solids. As soon as a safe ignition temperature of hydrogen is reached

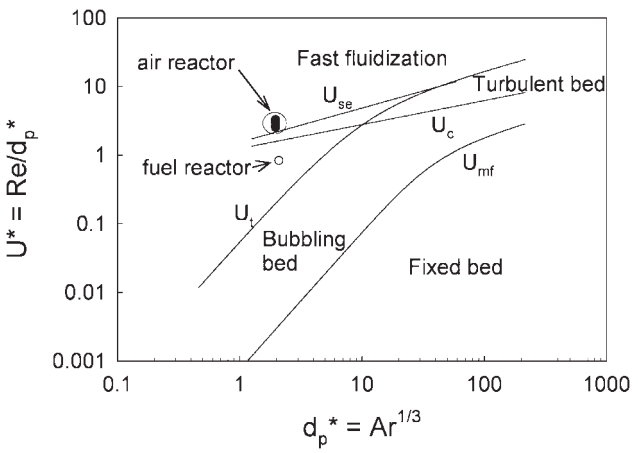

Figure 6. Fluidization regime of air and fuel reactor in the flow regime map suggested by Bi and Grace[47] at design load (120 kW fuel power with CH_4 as fuel); range shown for air reactor corresponds to a variation in the global air ratio from 1.05 to 1.30.

(i.e., at about 700 K), the fuel reactor fluidization is changed to nitrogen and H_2 is gradually added to the N_2 stream in order to increase the heat input. At about 1000 K, when the ignition of propane can be expected even in the particle-rich environment, propane is supplied to the air reactor through a separate nozzle. The start-up burner may be switched off as soon as fuel combusts in the air reactor and rapid further heating to the desired operating temperature is possible. The additional fuel to the air reactor may be switched to natural gas at temperatures above 1050 K in the air reactor. As soon as the operating temperature of 1100–1200 K is reached, the loop seal fluidization is switched to steam and the desired fuel is fed to the fuel reactor. If the oxygen carrier is active enough, the additional fuel to the air reactor can be completely turned off and the cooling system activated and adjusted in order to maintain the desired temperature. The whole startup procedure lasts about 2.5 h for the NiO-based carrier used in this study.

During operation, stable points are maintained for a sufficiently long time to assume steady state conditions. The operating parameters varied within the present study are temperature and fuel power input. All air is introduced into the air reactor at the primary fluidization level. The global air/fuel ratio is kept constant at a value of 1.1 throughout the tests. This means that the unit is operated at a lower air/fuel ratio compared to the design value of 1.2 reported in Table 2. Also, the total solids inventory is kept constant at 65 kg. As soon as steady state conditions (i.e., steady temperature and gas composition trends) prevail for at least 20 min and the online gas chromatograph has taken a gas sample for analysis, solids samples are taken out of both the upper and the lower loop seal more or less simultaneously to fully characterize the operating point. Then, the operating parameters (fuel power, air/fuel ratio, etc.) are set for the next point and the cooling system is adjusted in order to maintain the desired operating temperature.

For shutdown, the fluidization of the fuel reactor is first switched to nitrogen. As soon as all fuel has left the installation the post combustion may be turned off and fluidization is changed to air throughout the system. At a system temperature of about 600 K, the fluidization rates are reduced and the installation is left to cool slowly overnight.

The evaluation of experimental data is done using a comprehensive mass and energy balance model of the laboratory setup. The evaluation procedure is described in more detail by Bolhàr-Nordenkampf et al.[50]

Oxygen carrier and operating range

The oxygen carrier particles used have been manufactured from commercially available raw materials by VITO, Belgium, under the guidance of Chalmers University of Technology, Sweden. In all experiments presented below, a 50:50 mixture of two slightly different materials is used. The first oxygen carrier (VITO) is based on NiO and Al_2O_3. After sintering, the particles consist of inert $NiAl_2O_4$ and free NiO. The ingredients of the second oxygen carrier (VITOMg) are NiO, Al_2O_3, and MgO. These particles are also sintered to yield $MgAl_2O_4$, $NiAl_2O_4$, and free NiO. Further information on the particles and results of long-term integrity testing using these materials has recently been published by Linderholm et al.[51] (Table 3).

Table 3. Properties of the Oxygen Carrier Mixture Used (According to Linderholm et al.[51])

Meter	Unit	Value
Oxygen carrier		Ni/NiO
Active NiO content	%	40
Oxygen transport capacity R_0	kg/kg	0.087
Mean particle size	mm	0.135
Apparent density	kg/m^3	3416
Sphericity	–	0.9

Table 4. Experimental Operating Parameters

Parameter	Unit	Standard Value	Variation
Total solids inventory	kg	65	–
Fuel load	kW	140	60–140
Global air/fuel ratio	–	1.1	–
Fuel reactor temperature	K	1173	1073–1223

The results presented in this article will concentrate on an experimental campaign using the particle mixture described earlier. In a first run, the fuel reactor operating temperature was varied while fuel load and global stoichiometric air/fuel ratio were kept constant. Temperature variation was carried out starting from the lowest temperature and proceeding stepwise to the highest temperature. In a second run, a variation in the fuel load was performed at constant fuel reactor temperature and constant global air/fuel ratio. Here, the first point operated was at maximum load followed by a stepwise decrease toward the lowest load point addressed. The operating range investigated is summarized in Table 4.

Results and Discussion

Solids distribution in the system

The solids distribution in the fluidized bed system can be characterized using measured pressure profiles. The system pressure in vertical sections is dominated by the cumulative weight of solids above the measurement point. Figure 7 reports the full pressure profile in the system for the standard operating point according to Table 4. The air reactor shows a typical distribution for a fast fluidized riser. In the fuel reactor, most of the inventory is found in the bottom region with a steep decay towards the top of the reactor. This means that the upper part of the fuel reactor is still relatively lean in particles and the entrainment of the fuel reactor is lower compared to the air reactor. From the perspective of actual solids distribution in the system, more material is present in the fuel reactor compared to the air reactor. At the loop seals there are two measurement points located in each leg at the same height (about 0.1 m above the loop seal fluidization level). The pressure differences between these points reflect the wall friction of the particles flowing through the loop seal. Whereas the upper and lower loop seals show significant pressure drops in the direction of solids flow, the pressure drop for the fuel reactor internal loop seal is much smaller, indicating a lower rate of solids circulation in the fuel reactor internal loop compared to the global loop.

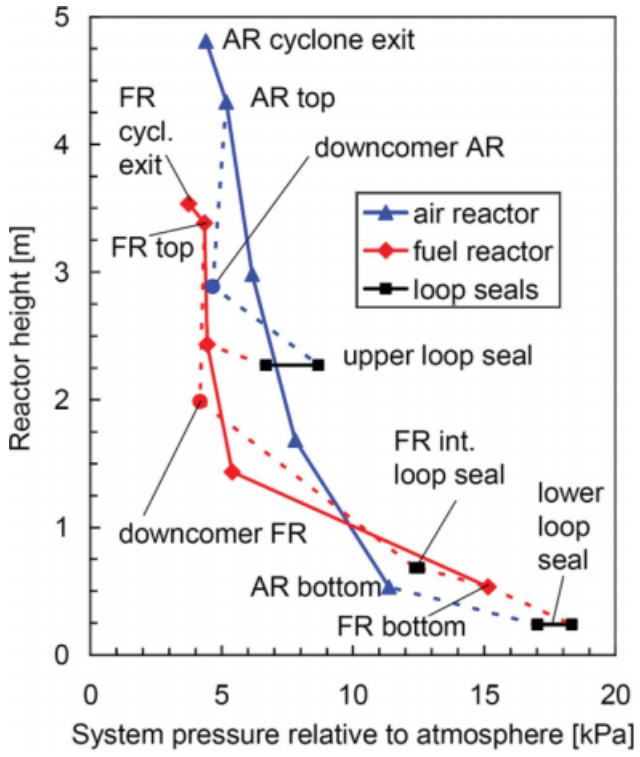

Figure 7. Pressure profile measured at 140 kW fuel power, a global air/fuel ratio of 1.1, and all air reactor fluidization to the primary level.

[Color figure can be viewed in the online issue, which is available at www.interscience.wiley.com.]

The solids distribution is expected to change with changes in gas velocities. This is expressed in terms of the pressure profiles during the load variation. Because the global air/fuel ratio is kept constant, the gas velocities in the air reactor and fuel reactor are proportional to fuel power. The air reactor profiles are drawn in Figure 8. For the purpose of comparison, the pressure differences relative to the pressure tap in the top of the air reactor are shown. It turns out that the solids inventory in the air reactor decreases with increasing load. At low loads, the solids tend to be concentrated in the lower part of the air reactor as expected. The fuel reactor profiles relative to the pressure at the top of the fuel reactor in Figure 9 show that the fuel reactor inventory has a tendency to increase with increasing load, but only up to the operating point at 100 kW fuel power. The shape of the fuel reactor profile reflects the rather weak development of the fast fluidized bed regime even at 140 kW. The material shift from the air reactor to the fuel reactor with increasing load can be explained by the solids flow resistance of the lower loop seal. This is in agreement with cold flow model results.[45] Obviously, however, the fuel reactor inventory increases less than the air reactor inventory decreases. Above 100 kW, no further increase in the fuel reactor inventory is found at all. The reason is most likely that with increasing fuel power, an increasing amount of particles are present between the reactors (i.e., in cyclones and downcomers).

The so-called "active solids inventory" m_{act} is calculated from the pressure difference Δp_{riser} between the reactor bottom and top according to

$$m_{act} = \frac{A_{riser} \cdot \Delta p_{riser}}{g} \tag{3}$$

with the riser cross section A_{riser} and gravity acceleration g. The active solids inventories of both air reactor and fuel reactor for the power variation are shown in Figure 10. Also, on the right-hand side of the y-axis in Figure 10, the specific solids inventory relative to fuel power is shown. The specific inventory is a relevant quantity with respect to estimation of large scale particle requirements. Fuel reactor inventories below 200 kg/MW are reached during these runs.

Global solids circulation

From solids samples taken at each stable point from the upper and the lower loop seal, i.e., at the solids inlet and outlet of both air reactor and fuel reactor, the global solids circulation rate can be assessed with great accuracy. The solids conversion is calculated from the difference between the fresh sample mass m and the sample mass in fully oxidized state m_{ox} using the theoretical oxygen transport capacity R_0 according to Table 3:

$$X_s = \frac{m - m_{ox} \cdot (1 - R_0)}{m_{ox} \cdot R_0} \tag{4}$$

This means that X_S is equal to zero in the fully reduced state and equal to one in the fully oxidized state. The temperature difference between the fuel reactor inlet and

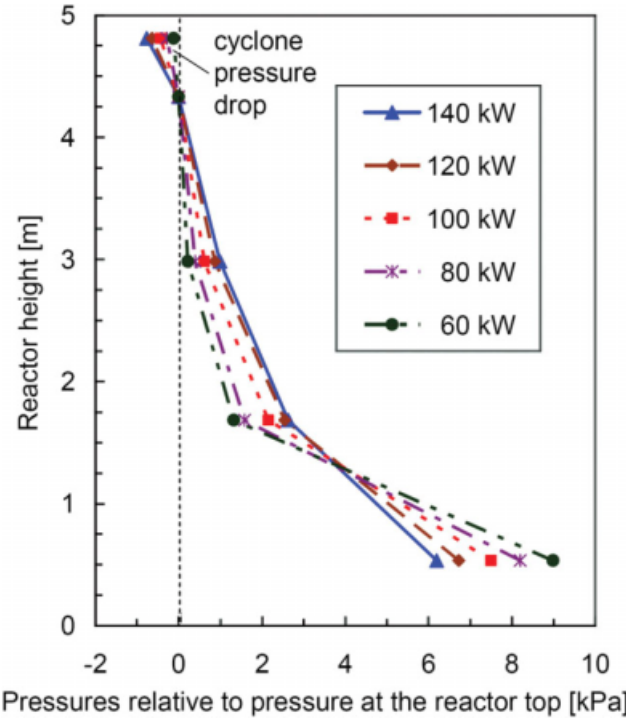

Figure 8. Pressure profiles along the air reactor during variation of fuel power (i.e., total gas flow rates).

[Color figure can be viewed in the online issue, which is available at www.interscience.wiley.com.]

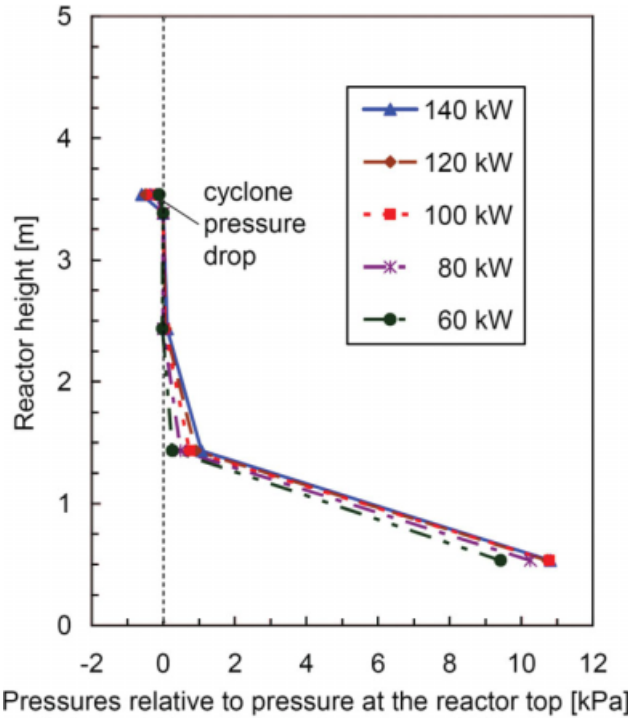

Figure 9. Pressure profiles along the fuel reactor during variation of fuel power (i.e., gas flow rates).

[Color figure can be viewed in the online issue, which is available at www.interscience.wiley.com.]

outlet could also be used for determination of solids circulation (since the fuel reactor is adiabatic). However, due to the extremely high solids circulation, this temperature difference is too low for reliable evaluation (only 5–15 K).

The global solids circulation can be determined from the measured degree of oxidation at the two sample points, global fuel conversion data, and fuel mass flow[49] and is shown in Figure 11, again for the power variation run. Secondary axes show the net solids flux in the air reactor, which is proportional to the circulation rate, and the ratio of air reactor exit velocity to the terminal velocity of the particles, which is proportional to the fuel power operated. As expected, the air reactor entrainment increases with increasing velocity. The oxygen carrier conversion states from the air reactor and fuel reactor are also shown in Figure 11. The mean solids conversion difference between air reactor and fuel reactor $\Delta X_S = X_{S,ULS} - X_{S,LLS}$ is a result of the total amount of oxygen transported and of the solids circulation rate. It decreases with increasing load from about 0.13 at 60 kW down to 0.07 at 140 kW. A very interesting parameter is the global level of the solids conversion state in the system (i.e., the average of $X_{S,ULS}$ and $X_{S,LLS}$). It is the result of a dynamic equilibrium governed by the apparent reaction rates faced in each of the reactors. If the reaction is very fast (or if the contact time is sufficiently long) in one of the reactors, the particles will tend to leave this reactor fully converted. If both apparent reaction rates are of the same order of magnitude, the solids conversion states may take intermediate values. The tendency toward lower global oxidation states at higher load means that the apparent reaction rate in the air reactor gets slower compared to the fuel reactor reaction rate. This could be attributed to the shift in solids inventory from air reactor to fuel reactor with increasing load according to Figure 10. However, the observations definitely leave room for further research. The steep transition in global oxidation state between the points at 60 and 80 kW fuel power (X_S = 0.7–0.8) and the points at 100–140 kW fuel power (X_S = 0.5–0.6) is currently not understood.

Fate of carbon and leakage assessment

It can be reported for all runs performed that no extra steam was added to the fuel reactor except for the loop seal fluidization, which amounts to a steam to CH_4 ratio of 0.2 to 0.4 in the worst case scenario that all loop seal steam would go to the fuel reactor. In reality, it is even likely that most of the lower loop seal steam is dragged toward the air reactor by the particle stream. Despite the practically pure CH_4 supply to the fuel reactor, no CO_2 has been detected from the air reactor under any conditions except in tests not shown here where fuel was deliberately added to the air reactor. This means that no carbon formation takes place and indeed 100% of the carbon ends up in the fuel reactor exhaust stream (also confirmed for operation of propane at a fuel power of 127 kW; air/fuel ratio 1.1). Moreover, a leakage of gas from the fuel reactor toward the air reactor can be excluded. Nitrogen measurements in the fuel reactor

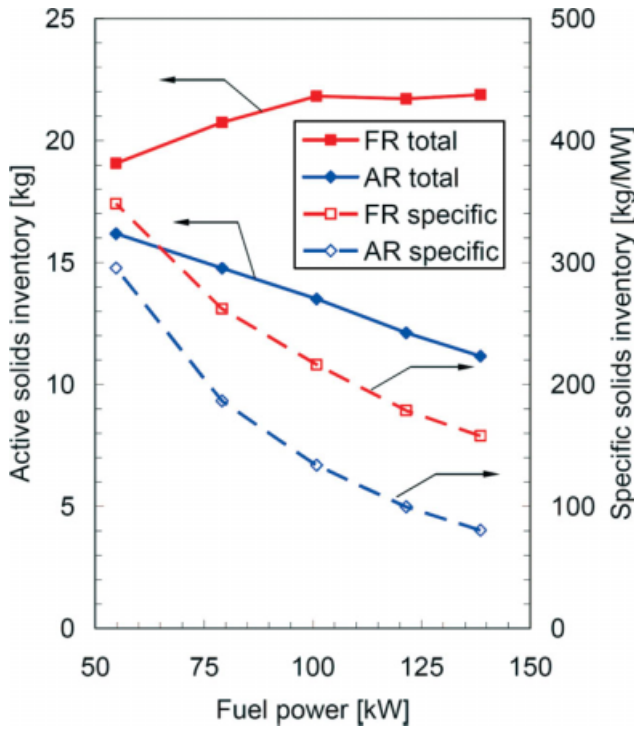

Figure 10. Active solids inventory as well as specific solids inventory in air reactor and fuel reactor vs. fuel power (i.e., gas flow rates).

[Color figure can be viewed in the online issue, which is available at www.interscience.wiley.com.]

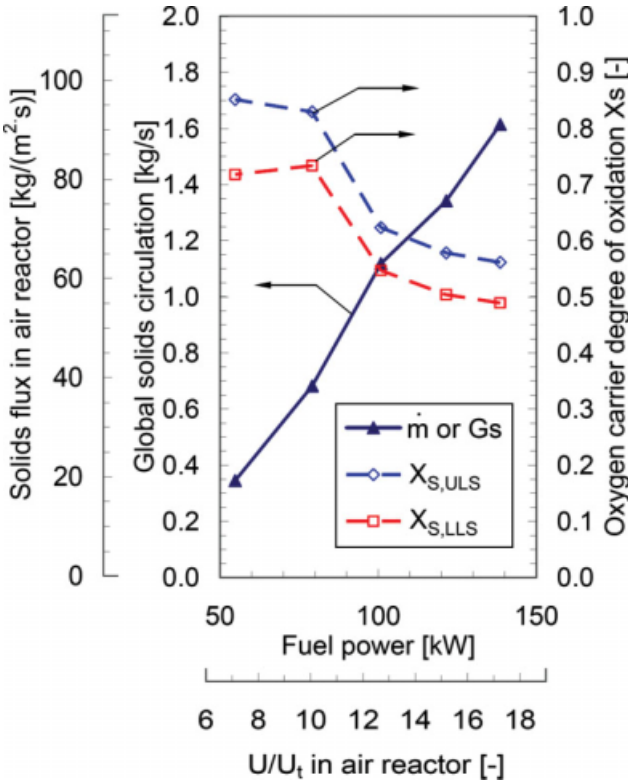

Figure 11. Global solids circulation rate and degree of oxygen carrier oxidation vs. fuel power. The specific solids flux in the air reactor and the ratio of air reactor exit velocity to the terminal velocity in the air reactor are shown as proportional axes.

[Color figure can be viewed in the online issue, which is available at www.interscience.wiley.com.]

exhaust stream indicate, however, that there is a small leakage from the air reactor into the fuel reactor. Such a leakage, also called "dilution (of the CO_2 stream)", can only be explained for the upper loop seal because the pressure situation would not allow gas convection from air reactor to fuel reactor in the lower loop seal (see Figure 7). An evaluation of the N_2 content in natural gas and in the fuel reactor exhaust suggests that 0.2–0.4 vol % of the gas supplied to the air reactor leaks into the fuel reactor. This means that about 0.5–1.2 vol % of the fuel reactor exhaust gas stream is contributed by dilution.

Chemical looping combustion performance

The performance of the chemical looping system in fuel conversion and CO_2 yield is a result of the characteristics of both the oxygen carrier and the reactor system. The fuel conversion is expressed for natural gas operation in terms of CH_4 conversion X_{CH_4} according to

$$X_{CH_4} = 1 - \left.\frac{y_{CH_4}}{y_{CO_2} + y_{CO} + y_{CH_4}}\right|_{\text{fuel reactor exhaust}} \quad (5)$$

where y_i represent gas phase mole fractions. The CO_2 yield γ_{CO_2} is based on the total carbon supplied to the fuel reactor and can be generally defined for operation of hydrocarbon fuels as

$$\gamma_{CO_2} = \left.\frac{y_{CO_2}}{y_{CO_2} + y_{CO} + \sum_i (x \cdot y_{C_xH_z})_i}\right|_{\text{fuel reactor exhaust}} \quad (6)$$

where i represents the different hydrocarbon species and x is the number of carbon atoms in a certain molecule. Expressions (5) and (6) are extremely convenient because only the gas analysis of the fuel reactor exhaust stream is needed and, furthermore, dry gas mole fractions can be directly applied (as measured). It is, however, important to notice that (5) and (6) can only be applied if carbon loss to the air reactor can be excluded.

Figure 12 shows the fuel conversion performance during the temperature variation run including an operating point with propane. It turns out that the CO_2 yield of the investigated oxygen carrier is strongly dependent on operating temperature. At lower temperatures the slip of unconverted fuel as CO and H_2 out of the fuel reactor is increased while the (primary) conversion of CH_4 seems to be less dependent on temperature. The CO_2 yield for propane operation indicates that the presence of higher hydrocarbons is not a problem in

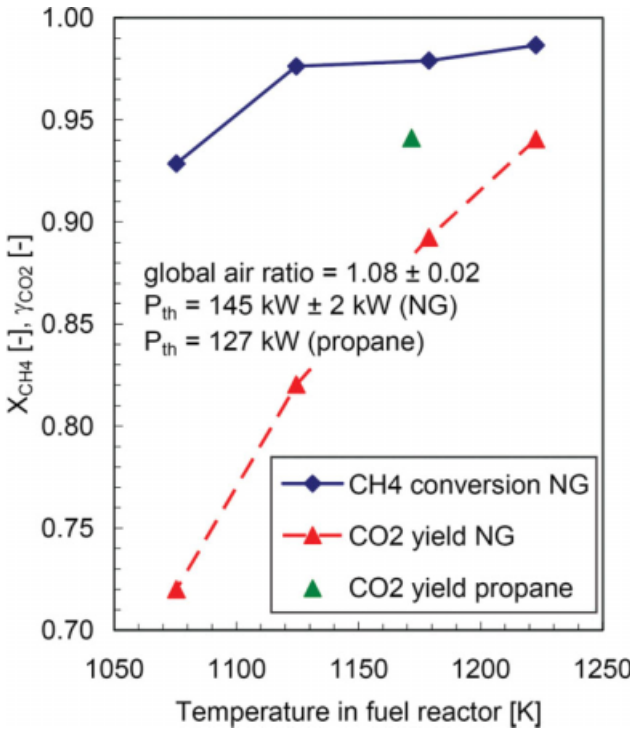

Figure 12. Methane conversion and CO_2 yield vs. fuel reactor operating temperature. Data from the temperature variation run (NG = natural gas).

[Color figure can be viewed in the online issue, which is available at www.interscience.wiley.com.]

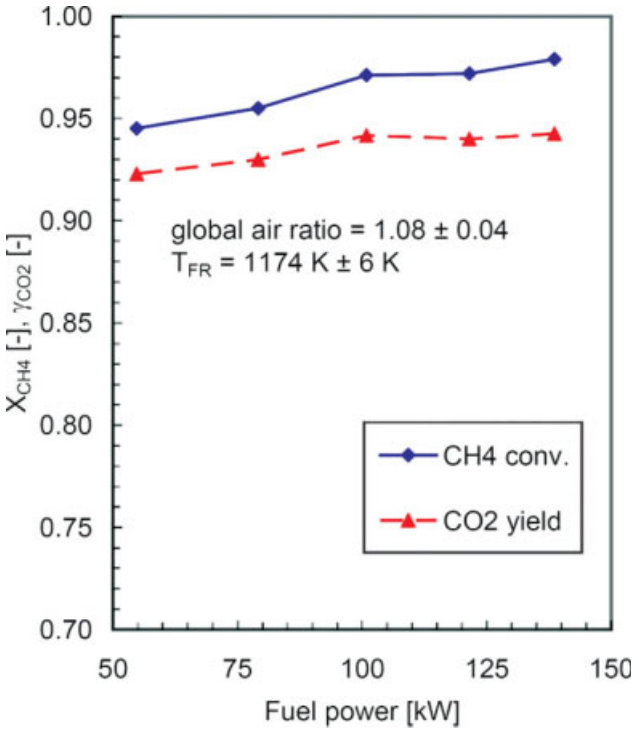

Figure 13. Methane conversion and CO_2 yield vs. fuel power. Data from the power variation run.

[Color figure can be viewed in the online issue, which is available at www.interscience.wiley.com.]

CLC. Contrarily, the CO_2 yield for C_3H_8 is even higher than for natural gas (CH_4) at the same temperature.

The fuel conversion performance of the system during the power variation run is reported in Figure 13. Here, a most interesting behavior of the investigated system is observed. The fuel conversion increases with increasing fuel power. A maximum is not reached within the investigated operating range. The most likely explanation for this behavior is that at increased fuel power, the increased gas–solids contact (due to the greater amount of solids present in the lean upper zone of the fuel reactor) over-compensates for the reduced gas phase residence times. It further means that there must be an operating point where the fuel conversion reaches a maximum. However, this point has not yet been reached within the present study. At this time, the limiting components of the installation are the natural gas compressor and the air reactor cooling system. It is important to mention that the optimum load depends on the reactivity of the oxygen carrier. For a less reactive oxygen carrier such as natural ilmenite, which was operated during hot commissioning of the unit, a clear decrease in fuel conversion with increasing fuel power was reported.[52]

Summarizing these results, it can be stated that the fluid dynamic behavior of the bench scale unit reflects expectations well. However, a somewhat lower fuel reactor cross section would have helped to obtain a more favorable solids distribution in the fuel reactor and thus would probably have increased the performance of the plant. Nevertheless, high fuel conversion is obtained with the NiO-based oxygen carrier in spite of the limited riser heights.

Conclusions

A system consisting of two circulating fluidized bed reactors hydraulically coupled by a loop seal in the bottom region of the two reactors is presented and investigated for chemical looping combustion using metal oxides for selective transport of oxygen. The proposed system is seen as a scale-up ready candidate for large scale chemical looping application. The main fluid dynamic characteristics expected are:

- high solids circulation rate
- low specific solids inventory
- stable solids distribution because of the hydraulic connection between the two reactors
- secondary reactor flow regime can be optimized with respect to gas phase conversion
- global solids circulation can be controlled by staged fluidization of the primary reactor or by controlling the flow resistance in the lower loop seal
- solids inventory can be shifted between the reactors by imposing moderate backpressure from the exhaust gas lines

The results obtained from the 120 kW bench scale unit give a clear proof of concept. The measured pressure profile indicates that the circulating fluidized bed regime in the primary reactor (air reactor) is well developed with particles distributed along the whole height. On the secondary reactor (fuel reactor) side, however, the particles are concentrated in the bottom region and only a low particle flow is indicated in the secondary reactor's internal loop.

Fuel conversion and CO_2 yield have been found to be well above 90% at relevant operating conditions for the NiO-based oxygen carrier. Since incomplete fuel conversion reduces the energy conversion efficiency of the combustor, measures for further improvement of fuel conversion are necessary. With NiO-based carriers, fuel conversion is also limited by thermodynamics. A final oxygen polishing step introducing pure oxygen in the fuel reactor exhaust gas stream can be a solution in large scale CLC applications. For the investigated oxygen carrier, a significant temperature dependency of CO_2 yield has been found.

The most interesting result with respect to the overall system performance is that fuel conversion increases with increasing fuel power at least up to 140 kW (natural gas). This means that the gas–solids contact in the fuel reactor improves with increasing load and this effect over-compensates for the effect of reduced gas phase residence times.

Generally, a design with higher riser reactors is expected to significantly improve global fuel conversion in the dual circulating fluidized bed system for CLC. Therefore, a scale-up step to a small scale demonstration size of about 10–50 MW fuel power seems feasible based on the present findings. Such an installation could potentially be run commercially as an industrial steam generator with CO_2 capture and could pave the way for further scale-up to sizes relevant for power generation.

Acknowledgments

This work is part of the EU financed project CLC GAS POWER (FP6 Contract No. 019800), coordinated by Chalmers University of Technology. The project is also part of Phase II of CCP (CO_2 Capture Project) through Shell.

Notation

A = cross section, m^2
g = gravitational acceleration, m s^{-2}
G_s = solids flux, kg m^{-2} s^{-1}
m = mass, kg
$\dot{m}$ = mass flow, kg s^{-1}
p = pressure, Pa
P_{th} = fuel power, W
R_0 = oxygen transport capacity (mass specific), kg kg^{-1}
T = temperature, K
U = superficial velocity, m s^{-1}
U_c = (superficial) velocity limit toward turbulent fluidization, m s^{-1}
U_{mf} = minimum fluidization (superficial) velocity, m s^{-1}
U_{se} = (superficial) velocity limit toward fast fluidization, m s^{-1}
U_t = terminal (superficial) velocity, m s^{-1}
x = stoichiometry of carbon in species
X = chemical conversion based on initial quantity
X_S = solids conversion (i.e., degree of oxidation)
y = mole fraction in gas phase, mol mol^{-1}

Greek letters

γ = chemical yield
Δ = symbolizes difference

Indices

AR = air reactor
act = active (i.e., actual) solids inventory
FR = fuel reactor
i = refers to chemical species
LLS = lower loop seal (from FR to AR)
riser = refers to fast fluidized bed reactor
ULS = upper loop seal (from AR to FR)

Literature Cited

1. Lyon RK, Cole JA. Unmixed combustion: an alternative to fire. *Combust Flame*. 2000;121:249–261.
2. Bolland O. Fundamental thermodynamic approach for analysing gas separation energy requirement for CO_2 capture processes. In: *Proceedings of the 8th International Conference on Greenhouse Gas Control Technologies (GHGT-8)*, Trondheim, Norway, 2006. Available at: folk.ntnu.no/obolland/pdf/GHGT8_Review_Lecture_Olav_Bolland.pdf.
3. Hossain MM, Lasa HI de. Chemical-looping combustion (CLC) for inherent CO_2 separations—a review. *Chem Eng Sci*. 2008;63:4433–4451.
4. Lyngfelt A, Thunman H. *Chemical-looping combustion: design, construction and 100 h of operational experience of a 10 kW prototype*. In: Thomas D, editor. *Carbon Dioxide Capture for Storage in Deep Geologic Formations—Results from the CO_2 Capture Project: Vol. 1—Capture and Separation of Carbon Dioxide from Combustion*. London: Elsevier, 2004. ISBN 0080445705.
5. Ryu HJ, Jin GT, Yi CK. Demonstration of inherent CO_2 separation and no NOx emission in a 50kWth chemical-looping combustor: continuous reduction and oxidation experiment. In: *Seventh International Conference on Greenhouse Gas Control Technologies (GHGT-7)*; Vancouver, Canada, September 5–9, 2004:1907–1910.
6. Johansson E, Mattisson T, Lyngfelt A, Thunman H. Combustion of syngas and natural gas in a 300 W chemical-looping combustor. *Chem Eng Res Des*. 2006;84:819–827.
7. Adánez J, Gayán P, Celaya J, De Diego LF, García-Labiano F, Abad A. Chemical looping combustion in a 10 kWth prototype using a CuO/Al_2O_3 oxygen carrier: effect of operating conditions on methane combustion. *Ind Eng Chem Res*. 2006;45:6075–6080.
8. Jukkola G, Levasseur A, Turek D, Teigen B, Jain S, Thibeault P. Performance results with ALSTOM's circulating moving bed combustor™. In: *Proceedings of the International Conference on Fluidized Bed Combustion*, Jacksonville, FL, May 18–21, 2003:99–105.
9. Lewis WK, Gilliland ER. Production of pure carbon dioxide. U.S. Patent 2,665,972, 1954.
10. Knoche KF, Richter H. Verbesserung der Reversibilität von Verbrennungsprozessen, *Brennstoff-Wärme-Kraft*. 1968;20:205–210 (in German).
11. Richter H, Knoche KF. Reversibility of combustion processes, efficiency and costing. Second Law analysis of processes. *ACS Symp Ser*. 1983;235:71–85.
12. Ishida M, Zheng D, Akehata T. Evaluation of a chemical-looping-combustion power-generation system by graphic exergy analysis. *Energy*. 1987;12:147–154.
13. Ishida M, Jin H. A novel combustor based on chemical-looping reactions and its reaction kinetics. *J Chem Eng Jpn*. 1994;27:296–301.
14. Ishida M, Jin H. A new advanced power-generation system using chemical-looping combustion. *Energy*. 1994;19:415–422.
15. Ishida M, Jin H. CO_2 recovery in a power plant with chemical looping combustion. *Energy Conversion Manage*. 1997;38 (Suppl 1): 187–192.
16. Lyngfelt A, Leckner B, Mattisson T. A fluidized bed combustion process with inherent CO_2 separation, application of chemical looping combustion. *Chem Eng Sci*. 2001;56:3101–3113.
17. Wolf J, Anheden M, Yan J. Performance analysis of combined cycles with chemical looping combustion for CO_2 capture. In: *Proceedings of 18th Pittsburg Coal Conference*, Newcastle, NSW, Australia, Session 23, December 3–7, 2001.
18. Ryu H-J, Bae D-H, Jin G-T. Chemical-looping combustion process with inherent CO_2 separation; reaction kinetics of oxygen carrier particles and 50kWth reactor design. In: *The World Congress of Korean and Korean Ethnic Scientists and Engineers*, Seoul, Korea, 2002:738–743.
19. Leion H, Mattisson T, Lyngfelt A. Solid fuels in chemical-looping combustion. *Int J Greenhouse Gas Control*. 2008;2:180–193.
20. Johansson M, Mattisson T, Rydén M, Lyngfelt A. Carbon capture via chemical-looping combustion and reforming. In: *International seminar on carbon sequestration and climate change*, Rio de Janeiro, October 24–27, 2006.
21. Lyngfelt A, Johansson M, Mattisson T. Chemical looping combustion—status of development. In: Werther J, Nowak W, Wirth, KE, Hartge EU, editors. *Circulating Fluidized Bed Technology IX, TuTech*, Hamburg, Germany, 2008.
22. Hofbauer H, Rauch R, Löffler G, Kaiser S, Fercher E, Tremmel H. Six years experience with the FICFB gasification process. In: Palz W, Spitzer J, Maniatis K, Kwant K, Helm P, Grassi A, editors. *Twelfth European Biomass Conference*, ETA, Florence, Italy, 2002:982–985.
23. Kolbitsch P, Pröll T, Bolhàr-Nordenkampf J, Hofbauer H. Design of a chemical looping combustor using a dual circulating fluidized bed reactor system. *Chem Eng Technol*. 2009;32:398–403.
24. Grace JR. High-velocity fluidized bed reactors. *Chem Eng Sci*. 1990;45:1953–1966.
25. Bridgwater AV. The technical and economic feasibility of biomass gasification for power generation. *Fuel*. 1995;14:631–653.
26. Hofbauer H, Stoiber H, Veronik G. Gasification of organic material in a novel fluidised bed system. In: *Proceedings of the First SCEJ Symposium on Fluidisation*, The Society of Chemical Engineers, Tokyo, Japan. 1995:291–299.
27. Paisley MA, Farris MC, Black JW, Irving JM, Overend RP. Preliminary operating results from the Battelle/FERCO gasification demonstration plant in Burlington, Vermont, USA. In: Kyritsis S, Beenackers A, Helm P, Grassi A, Chiaramonti D, editors. *First World Conference on Biomass for Energy and Industry, Eleventh EC and First World Conference, Vol. 2,* Sevilla, Spain, June 5–9, 2000. London: James & James Ltd. 2001:1494–1497.
28. Corella J, Toledo JM, Molina G. A review on dual fluidized-bed biomass gasifiers. *Ind Eng Chem Res*. 2007;46:6831–6839.
29. Xu G, Murakami T, Suda T, Matsuzaw Y, Tani H. Two-stage dual fluidized bed gasification: its conception and application to biomass. *Fuel Process Technol*. 2009;90:137–144.
30. Han C, Harrison DP. Simultaneous shift reaction and carbon dioxide separation for the direct production of hydrogen. *Chem Eng Sci*. 1994;49:5875–5883.
31. Lin SY, Suzuki Y, Hatano H, Harada M. Developing an innovative method, HyPr-RING, to produce hydrogen from hydrocarbons. *Energy Conversion Manage*. 2002;43:1283–1290.
32. Johnsen K, Ryu HJ, Grace JR, Lim CJ. Sorption-enhanced steam reforming of methane in a fluidized bed reactor with dolomite as CO_2-acceptor. *Chem Eng Sci*. 2006;61:1195–1202.

33. Pfeifer C, Puchner B, Hofbauer H. In-situ CO_2-absorption in a dual fluidized bed biomass steam gasifier to produce a hydrogen rich syngas. *Int J Chem React Eng*. 2007;5:A9. Available at: http://www.bepress.com/ijcre/vol5/A9.
34. Weimer T, Berger R, Hawthorne C, Abanades JC. Lime enhanced gasification of solid fuels: examination of a process for simultaneous hydrogen production and CO_2 capture. *Fuel*. 2008;87:1678–1686.
35. Florin NH, Harris AT. Review of enhanced hydrogen production from biomass with in situ carbon dioxide capture using calcium oxide sorbents. *Chem Eng Sci*. 2008;63:287–316.
36. Shimizu T, Hirama T, Hosoda H, Kitano K, Inagaki M, Tejima K. A twin fluid-bed reactor for removal of CO_2 from combustion processes. *Chem Eng Res Des*. 1999;77:62–68.
37. Gupta H, Fan LS. Carbonation-calcination cycle using high reactivity calcium oxide for carbon dioxide separation from flue gas. *Ind Eng Chem Res*. 2002;41:4035–4042.
38. Abanades JC, Anthony EJ, Lu DY, Salvador C, Alvarez D. Capture of CO_2 from combustion gases in a fluidized bed of CaO. *AIChE J*. 2004;50:1614–1622.
39. Abanades JC, Anthony EJ, Wang J, Oakey JE. Fluidized bed combustion systems integrating CO_2 capture with CaO. *Environ Sci Technol*. 2005;39:2861–2866.
40. Romeo LM, Abanades JC, Escosa JM, JM, Paño J, Giménez A, Sánchez-Biezma A, Ballesteros JC. Oxyfuel carbonation/calcination cycle for low cost CO_2 capture in existing power plants. *Energy Conversion Manage*. 2008;49:2809–2814.
41. Jukkola G, Liljedahl G, Nsakala NY, Morin J-X, Andrus H. An Alstom vision of future CFB technology based power plant concepts. In: *Proceedings of the 18th International Conference on Fluidized Bed Combustion*, Art. no. FBC2005–78104, American Society of Mechanical Engineers (ASME), Toronto, Canada. 2005:109–120.
42. Andrus HE, Thibeault PR, Jain SC. Alstom's hybrid combustion-gasification chemical looping technology development—Phase II. In: *Proceedings of the 23rd Annual International Pittsburgh Coal Conference*, Pittsburgh, PA, September 26, 2006.
43. Andrus H. Chemical looping combustion—R&D efforts by Alstom. In: *IEA GHG Second Workshop of the International Oxy-Combustion Research Network*, Windsor, CT, January 25–26, 2007.
44. Kolbitsch P, Pröll T, Bolhàr-Nordenkampf J, Hofbauer H. Operating experience with chemical looping combustion in a 120 kW dual circulating fluidized bed (DCFB) unit. In: *Ninth International Conference on Greenhouse Gas Control Technologies (GHGT-9)*, Washington D.C. Available at: http://www.co2captureproject.com/ghgt-9/GHGT9_Kolbitsch.pdf.
45. Pröll T, Rupanovits K, Kolbitsch P, Bolhàr-Nordenkampf J, Hofbauer H. Cold flow model study on a dual circulating fluidized bed system for chemical looping processes. *Chem Eng Technol*. 2009;32:418–424.
46. Kolbitsch P, Pröll T, Hofbauer H. Modeling of a 120 kW chemical looping combustion reactor system using a Ni-based oxygen carrier. *Chem Eng Sci*. 2009;64:99–108.
47. Bi HT, Grace JR. Flow regime diagrams for gas-solid fluidization and upward transport. *Int J Multiphase Flow*. 1995;21:1229–1236.
48. Hugi E, Reh L. Design of cyclones with high solids entrance loads. *Chem Eng Technol*. 1998;21:716–719.
49. Kolbitsch P, Bolhàr-Nordenkampf J, Pröll T, Hofbauer H. Characterization of chemical looping pilot plant performance via experimental determination of solids conversion. *Energy Fuels*. 2009;23:1450–1455.
50. Bolhàr-Nordenkampf J, Pröll T, Kolbitsch P, Hofbauer H. Comprehensive modeling tool for chemical looping based processes. *Chem Eng Technol*. 2009;32:410–417.
51. Linderholm C, Mattisson T, Lyngfelt A. Long-term integrity testing of spray-dried particles in a 10 kW chemical-looping combustor using natural gas as fuel. *Fuel*. 2009;88:2083–2096.
52. Pröll T, Mattisson T, Mayer K, Bolhàr-Nordenkampf J, Kolbitsch P, Lyngfelt A, Hofbauer H. Natural minerals as oxygen carriers for chemical looping combustion in a dual circulating fluidized bed system. *Energy Procedia*. 2009;1:27–34.

Manuscript received Jan. 15, 2009, and revision received Apr. 1, 2009.